

See discussions, stats, and author profiles for this publication at: <https://www.researchgate.net/publication/260913309>

# Conformal Cytocompatible Ferrite Coatings Facilitate the Realization of a Nanovoyager in Human Blood

ARTICLE *in* NANO LETTERS · MARCH 2014

Impact Factor: 13.59 · DOI: 10.1021/nl404815q · Source: PubMed

---

CITATIONS

18

READS

92

## 6 AUTHORS, INCLUDING:



Pooyath Lekshmy Venugopalan

Indian Institute of Science

3 PUBLICATIONS 46 CITATIONS

[SEE PROFILE](#)



Yashoda Chandorkar

Indian Institute of Science

4 PUBLICATIONS 40 CITATIONS

[SEE PROFILE](#)



Srinivasrao Shivashankar

Indian Institute of Science

202 PUBLICATIONS 1,677 CITATIONS

[SEE PROFILE](#)

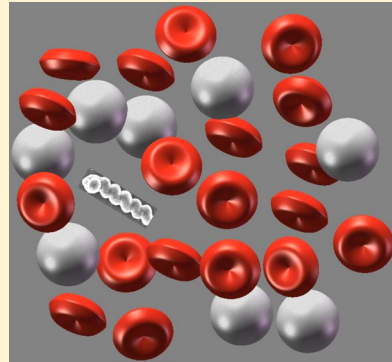
# Conformal Cytocompatible Ferrite Coatings Facilitate the Realization of a Nanovoyager in Human Blood

Pooyath Lekshmy Venugopalan,<sup>\*,†</sup> Ranajit Sai,<sup>‡</sup> Yashoda Chandorkar,<sup>‡</sup> Bikramjit Basu,<sup>‡</sup> Srinivasrao Shivashankar,<sup>†,‡</sup> and Ambarish Ghosh<sup>\*,†,§,⊥</sup>

<sup>†</sup>Centre for Nano Science and Engineering, <sup>‡</sup>Materials Research Centre, <sup>§</sup>Department of Electrical Communication Engineering, <sup>⊥</sup>Department of Physics, Indian Institute of Science, Bangalore 560012, India

## Supporting Information

**ABSTRACT:** Controlled motion of artificial nanomotors in biological environments, such as blood, can lead to fascinating biomedical applications, ranging from targeted drug delivery to microsurgery and many more. In spite of the various strategies used in fabricating and actuating nanomotors, practical issues related to fuel requirement, corrosion, and liquid viscosity have limited the motion of nanomotors to model systems such as water, serum, or biofluids diluted with toxic chemical fuels, such as hydrogen peroxide. As we demonstrate here, integrating conformal ferrite coatings with magnetic nanohelices offer a promising combination of functionalities for having controlled motion in practical biological fluids, such as chemical stability, cytocompatibility, and the generated thrust. These coatings were found to be stable in various biofluids, including human blood, even after overnight incubation, and did not have significant influence on the propulsion efficiency of the magnetically driven nanohelices, thereby facilitating the first successful “voyage” of artificial nanomotors in human blood. The motion of the “nanovoyager” was found to show interesting stick–slip dynamics, an effect originating in the colloidal jamming of blood cells in the plasma. The system of magnetic “nanovoyagers” was found to be cytocompatible with C2C12 mouse myoblast cells, as confirmed using MTT assay and fluorescence microscopy observations of cell morphology. Taken together, the results presented in this work establish the suitability of the “nanovoyager” with conformal ferrite coatings toward biomedical applications.



**KEYWORDS:** Artificial nanomotors, Magnetic propellers, Nanovoyagers, Cytotoxicity, Conformal Ferrite coating, Human blood

## INTRODUCTION

The idea of tiny vessels roaming around in human blood vessels working as surgical nanorobots was first proposed by Richard Feynman:<sup>1</sup> a vision that has triggered imagination<sup>2–4</sup> in scientists and nonscientists alike. With current advances in nanotechnology, there have been several strategies<sup>4–6</sup> to realize this dream of a “nanovoyager”, aiming to move artificial nanostructures in biological environments in a controllable manner. Of various methods of nanomanipulation, optical<sup>7</sup> and magnetic<sup>8</sup> tweezers are the oldest, requiring highly focused intense lasers or strong magnets in close vicinity of the nanostructures, and are therefore unsuitable for *in vivo* applications. More recent efforts toward building steerable nanomotors have, therefore, utilized alternate strategies, which can be divided into two wide classes. The first rely on powering the nanomotors through chemical means, among which self-electrophoretic<sup>9,10</sup> and bubble-driven<sup>11,12</sup> propulsion methods are most commonly used. These and most other examples of chemically powered motors suffer from an important drawback: toxic chemicals like hydrogen peroxide ( $H_2O_2$ ) and hydrazine<sup>13</sup> derivatives are the commonly used fuels, which are inherently incompatible with living systems. Water-driven<sup>14</sup> motors, which do not require  $H_2O_2$  as the fuel, are promising, but their lifetime is strongly dependent on the composition of the media.

The second class of nanomotors is powered by physical means, where the source of power could include electric,<sup>15</sup> magnetic,<sup>16–23</sup> or acoustic<sup>13,24,25</sup> fields. Of these various techniques, magnetically driven nanomotors are actuated by small homogeneous magnetic fields (typically tens of gauss), typically rotating at frequencies less than 100 Hz. This can be achieved even in large Helmholtz coils (on the scale of meters); implying magnetic propulsion is highly suitable for practical *in vivo* applications. Electrical and acoustic methods are also promising, although their suitability in practical applications would depend on the power levels required to operate them under *in vivo* conditions. As far as we are aware, this has not yet been discussed in the literature. In spite of such promising technologies, most magnetically or acoustically driven nanomotors have so far been actuated in deionized water and, in a few cases, in media of biological relevance, such as serum.<sup>20,24,26</sup> The questions then arise: why has there not been any demonstration of an artificial nanomotor being driven in unmodified human blood, and what are the steps to be taken to achieve the same?

**Received:** December 29, 2013

**Revised:** March 17, 2014

**Published:** March 19, 2014

The only reported attempt to maneuver a nanovoyager in human blood has been with catalytic microjets,<sup>27</sup> which were moved in human blood diluted 10× with H<sub>2</sub>O<sub>2</sub> at physiological temperatures (37 °C). The lower viscosity of blood at these elevated temperatures was critical<sup>28</sup> for the success of this experiment, along with the requirement that the concentration of the red blood cells and the serum be significantly reduced. On the other hand, there has not been a successful voyage of physically driven (magnetic or acoustic) nanomotors in blood. The first demonstration of magnetic- or ultrasound-powered microswimming in other biofluids (Fetal Bovine Serum<sup>20</sup>) was achieved with SU8-based helices, and more recently in human serum<sup>26</sup> and saliva.<sup>24</sup> As we show in this paper, for artificial nanomotors to be successfully maneuvered in undiluted human blood, two important experimental challenges need to be met: (1) The thrust generated by the propeller needs to be large enough to overcome the large drag due to the presence of the blood cells. (2) Many nanomotors, including the chemically and acoustically powered ones, contain a magnetic material which can be used for controlling their direction of motion. The large concentration of ions (chlorides, phosphates, etc.) in blood can etch most magnetic materials easily, which necessitates a conformal protective coating around the nanomotor. Although various coatings have been implemented in the literature, most of them work only for a short duration (~ less than one hour) in biological fluids, implying that the protection of the magnetic layer for a longer duration (~ overnight or more) is not trivial to achieve. Furthermore, it is important that the materials chosen in these studies are not toxic if *in vivo* studies are to be pursued.

## RESULTS AND DISCUSSION

As we demonstrate in this paper, it is possible to fabricate a system of magnetic nanovoyagers that can retain the magnetic properties in various biological fluids over extended periods of time (overnight or more), can generate enough thrust to propel in human blood, and with an appropriate choice of materials, can be made nontoxic as well. The method of fabrication to make helical shapes was based on GLAD (glancing angle deposition), which has been described extensively in the literature.<sup>29</sup> The helical nanostructures were typically made of SiO<sub>2</sub>, where a single evaporation on a 3 in. prepatterned wafer (further details in the Materials and Methods section) could yield more than 10<sup>9</sup> nanohelices (also referred to as nanopropellers<sup>18,30</sup>). As shown in Figure 1A, the wafer was sonicated in deionized water for a few minutes to disperse the nanohelices in solution and was subsequently laid down on another substrate. We deposited a magnetic material (e.g., cobalt, iron) on the helices and magnetized them such that their direction of magnetization was perpendicular to the long axis of the helices. Subsequently, we used different methods to obtain (achieve) a conformal coating of various materials around the magnetic material. The choice of coating materials and their thicknesses were partially inspired by existing literature, including (i) thermal evaporation of gold<sup>31</sup> (and silver), (ii) ALD (atomic layer deposition) of alumina, (iii) PECVD (plasma enhanced chemical vapor deposition) of SiO<sub>2</sub>, (iv) microwave-assisted, chemically synthesized zinc ferrite, and (v) sputtering of titanium.<sup>20</sup> The SEM image of a ferrite-coated propeller is shown later in the manuscript.

To check both the short- and long-term stability of the magnetic materials in various types of biological fluids, we followed a sequence of steps shown schematically in Figure 1B.

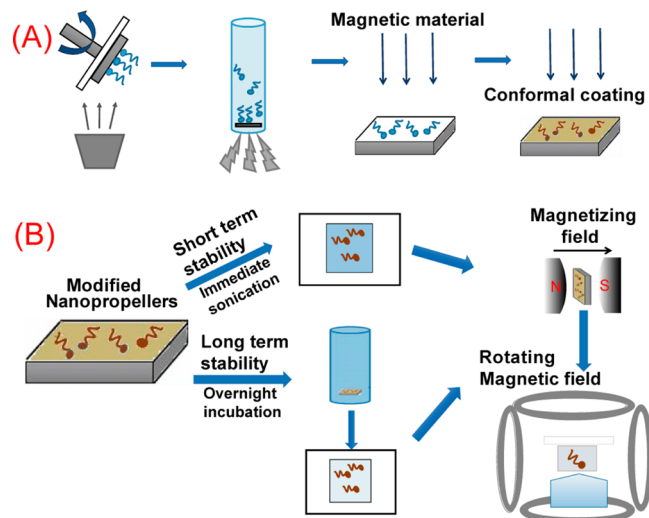


**Figure 1.** (A) Schematic of the fabrication process. (B) Method of checking the short- and long-term stability of the propellers in various biofluids. See main text for details.

For short-term studies, we sonicated the substrate containing the surface-modified (i.e., with protective coating) magnetized nanopropellers in three model biofluids, namely (i) phosphate-buffered saline (PBS), (ii) simulated body fluid (SBF), and (iii) foetal bovine serum (FBS) (details in the Materials and Methods section), with deionized water as the control. As the propellers were agitated off the substrate into the particular biofluid, we placed a small quantity (~ 5 μL) of the resulting suspension in a fluidic chamber inside a triaxial Helmholtz coil capable of producing rotating magnetic fields whose strength could be several tens of gauss and rotational frequency of around 100 Hz. The motion of the propellers was observed through an optical (bright-field) microscope integrated with the Helmholtz coil and, from the motion of the propellers, it was possible to differentiate between controlled magnetic actuation and random Brownian motion. The results of our short-term observations, which corresponded to about one hour, are shown in Table 1. Apart from zinc ferrite, no other coating could protect the magnetic layer for more than one hour. Among the various biofluids, the propellers could be actuated for a much longer duration in FBS than in SBF and PBS. It is interesting to note that the previous demonstrations of nanomotors were mostly in serum, both for acoustically and magnetically driven systems. The control experiment with deionized water showed the propellers can be actuated indefinitely, irrespective of the coating used.

For practical applications, it is necessary for the propellers to be stable in various types of biological fluids over extended periods of time, which was investigated by following a sequence of steps shown in Figure 1B. The substrates containing the modified propellers were incubated overnight in a particular biofluid, following which we investigated their dynamics under rotating magnetic fields. The results were similar to short-term studies (see Table 1) in which, except for the ferrite-coated propellers, all the other surface coatings were found to be incapable of protecting the magnetic films in PBS/SBF. This was further confirmed by EDS (energy dispersive X-ray spectrometry) analysis of the surface composition (see Table 1) of the incubated propellers, which clearly showed the superiority of the ferrite coating over the others. The EDS

**Table 1. Results of Short- and Long-Term Observations of Propellers with Various Coatings in Different Bio-Fluids<sup>a</sup>**

type of coating and thickness	response in PBS/SBF/FBS after overnight incubation	response time after direct sonication in PBS/SBF/FBS	EDS results for Co/Fe after incubation in PBS/SBF/FBS
evaporation Au: 100 nm	PBS/SBF: Nil	PBS/SBF: < 1 min.	PBS/SBF: 0% Co
ALD Alumina: 50 nm	FBS: 100%	FBS: > 1 h	FBS: > 99% Co
PECVD silica: 50 nm			
Ti sputtering: 100 nm			
zinc ferrite: 175 nm on Co coated propellers	PBS: 55% SBF: 95% FBS: 100%	PBS/SBF: > 1 h FBS: > 1 h	PBS: ~50% Co SBF: ~65% Co FBS: ~99% Co
zinc ferrite: 150 nm on Fe-coated propellers	PBS: 100% SBF: 100% FBS: 100%	PBS/SBF: > 1 h FBS: > 1 h	PBS: ~88% Fe SBF: ~92.5% Fe FBS: ~99% Fe
zinc ferrite: 50 nm on Co-coated propellers	PBS: 20% SBF: 50% FBS: 100%	PBS/SBF: > 1 h FBS: > 1 h	PBS: ~14% Co SBF: ~23% Co FBS: ~99% Co

<sup>a</sup>Also shown are the EDS results of the presence of magnetic material after overnight incubation.

study also revealed an advantage of using Fe over Co, as Fe was etched at a lower rate in PBS and SBF.

Although ferrite coatings allowed the system to achieve good chemical stability, it is important to ask whether the increase in thickness of the propellers due to the ferrite coating could affect their propulsion efficiency. The structural differences between the uncoated and the coated propellers can be seen in the SEM images shown in Figure 2A. To compare their propulsion

efficiencies, we have studied their linear translation speeds as a function of the frequency of the rotating magnetic field in deionized water. Two representative results are shown in Figure 2B. For both the propellers, the angle of magnetization was along the short axis, which implied a corkscrew type motion with a speed that increased linearly with frequency until the step-out frequency ( $\Omega_2$ ), beyond which the propellers could not rotate in sync with the rotating field and therefore slowed down. Because  $\Omega_2 \propto (mB/\eta)$ , where  $m$  is the magnitude of the magnetic moment,  $\eta$  is the viscosity of the surrounding fluid (here, water), and  $B$  is the strength of the magnetic field (3 G for both), the difference of  $\Omega_2$  (55 Hz for uncoated and 32 Hz for coated propellers) reflected the variability of the magnetic moment among different propellers (typical variation ~50%) and not related to the ferrite coating. A more interesting aspect was the hydrodynamic pitch of the propeller, defined as the ratio of the linear propulsion velocity to the rotational frequency of the applied torque (assuming frequency less than  $\Omega_2$ ), which was approximately the same between coated and uncoated propellers, implying similar propulsion efficiency. The measured pitch (~110 nm) was significantly lower than the geometrical pitch (~800 nm); however, it is possible to improve on the propulsion efficiency further by using a more optimized geometry as predicted by recent theoretical calculations.<sup>32</sup> Although the ferrite coatings did not affect the propulsion abilities in the helices presented here, the results may differ for optimized geometries.

Except when they were coated with the ferrite, we could observe a clear change in the appearance of the substrates after incubation in PBS/SBF (not in FBS), which was related to the loss of the magnetic layer. A very similar effect occurred when

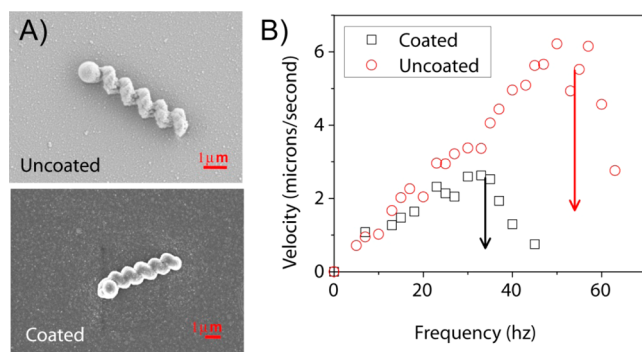


**Figure 2.** (A) SEM images of (top) uncoated propellers containing 65 nm Fe film on silica helices and (bottom) coated propellers with 175 nm conformal ferrite coating added to the uncoated propellers. (B) Translational speed versus rotational frequency of the magnetic field, both for coated and uncoated propellers in deionized water. The variation of the step-out frequency (marked with arrows) corresponds to the variability of the magnetic moment.

**Table 2. Results of Long- and Short-Term Observations of Propellers with Various Thicknesses of the Ferrite Coatings in Blood<sup>a</sup>**

type of coating and thickness	response in blood after overnight incubation	response time after direct sonication in blood	EDS results for Co/Fe after incubation in blood
zinc ferrite: 50 nm on Fe-coated propellers	100%	>1 h	85% Fe
zinc ferrite: 50 nm on Co-coated propellers	13%	>1 h	3% Co
zinc ferrite: 175 nm on Fe-coated propellers	100%	>1 h	>95% Fe
zinc ferrite: 175 nm on Co-coated propellers	25%	>1 h	10% Co

<sup>a</sup>Also shown are the EDS results of the presence of magnetic material after overnight incubation.

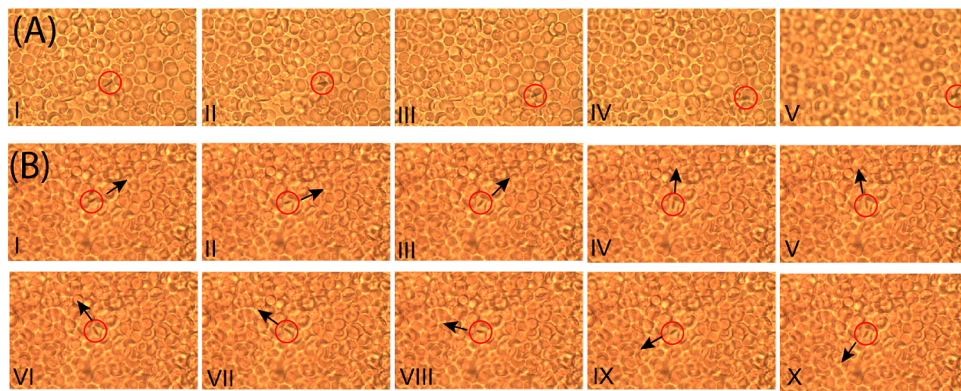


**Figure 3.** (A) Sequence of images taken from movie M1, where the propeller can be seen (marked with a circle) to travel through blood cells from left to right through a blood sample. The time lapse between successive images was approximately 2 s. (B) Sequence of images taken from M2, where the orientation of the rotating propeller has been marked clearly. The time lapse between successive images was approximately 0.015 s. The plane of rotation of the magnetic field was different for M2; see the main text for more details.

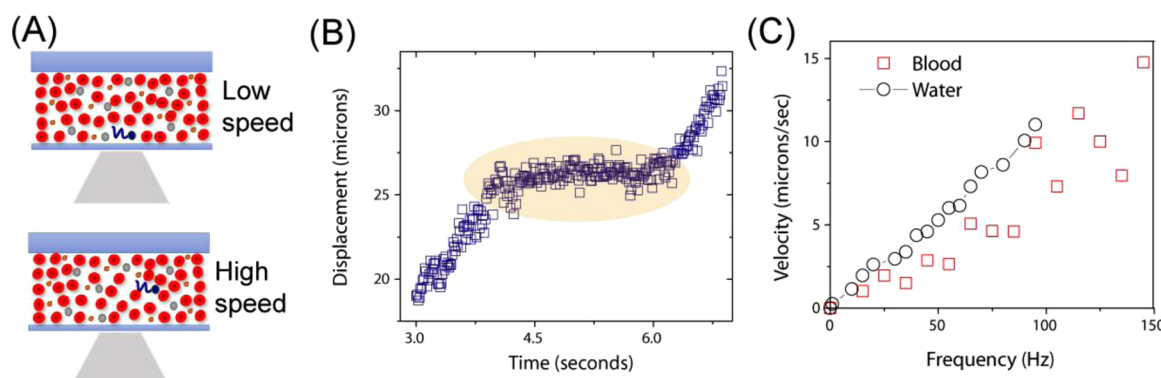


**Figure 4.** (A) Schematics for positions of the propellers in the experimental chamber. (B) Displacement versus time for magnetic field at 50 G and frequency 85 Hz for a propeller going through blood cells, for 1.8 $\times$  diluted blood (M4: corresponding movie). The stick-and-slip motion of the propeller going through the blood cells has been highlighted. (C) Velocity versus frequency for a propeller moving through the blood cells. Also shown in the same graph is the motion of the propellers in water.

the substrates (not the ferrite-coated ones) were placed in human blood, to which 2 mg/mL EDTA was added so as to prevent clotting under ambient conditions. This implied that the chemical composition of blood was significantly harsher than that of FBS, which is possibly why there have been nanovoyagers demonstrated in serum and FBS but not in undiluted blood. To investigate the chemical stability of the ferrite coated propellers in blood, we undertook an incubation study similar to what has been described before. The results (Table 2) clearly show the superior chemical stability of the ferrite coated propellers with iron as the underlying magnetic material.

To check the motion of ferrite-coated propellers, it was necessary to release them from the substrate into blood. However, to sonicate the substrates directly in blood would disrupt the blood cells. Accordingly, we sonicated the substrate in saline and then mixed it with fresh human blood (with EDTA). Upon application of rotating magnetic fields, the propellers (with ferrite coating on iron or cobalt) could be moved controllably through the blood cells suspended in the plasma. The back and forth motion of the propellers in the medium is demonstrated in the movie M1 in the Supporting Information, and a few frames from the movie are shown in Figure 3A. Apart from linear motion, it was also possible to rotate the propeller about its short axis, for which we magnetized the propeller to render the long axis the direction

of magnetization. The magnetic field was rotated in the image plane of the microscope, which resulted in the propeller rotating in the same plane. A sequence of images is shown in Figure 3B (see movie M2 in the Supporting Information). It is encouraging to note that the thrust generated by the ferrite-coated magnetic propellers not only was large enough to achieve corkscrew-type motion in blood but also rotates around its short axis at 40 Hz, which required overcoming higher viscous drag.

The experimental procedure required mixing a small amount of saline, which resulted in a slight dilution of the blood, which corresponded to 3 $\times$  and 4 $\times$  for the movies M1 and M2, respectively. The lowest dilution presented in this study (see Supporting Information movie M3) was 1.8 $\times$ ; however, for the entire range of dilutions (1.8 $\times$ –20 $\times$ ) studied during the course of this study, it was always possible to move the propellers in a controlled fashion, although the efficiency of propulsion had large variability (discussed later). It is easy to see that the system of magnetic nanovoyagers would work even if the saline-propeller suspension were mixed with a much larger quantity of blood, that is, a case where the blood is effectively undiluted, a case relevant to *in vivo* studies. The argument can be made based on the following reasoning: (i) The temperature of the experimental setup was around 25 °C, where the viscosity of the plasma is significantly higher than at physiological temperatures (37 °C). This implies that the

propellers would be subject to lower effective drag under *in vivo* conditions. (ii) Assuming the direction of magnetization was along the short axis<sup>33,34</sup> of the propeller, the step-out frequency ( $\Omega_2$ ) of the rotating magnetic field ( $B$ ), at which the propellers could not rotate in sync with the rotating field was proportional to  $\Omega_2 \propto (mB/\eta)$ , where  $m$  is the magnitude of the magnetic moment, and  $\eta$  is the viscosity of the surrounding fluid. In the experiments reported here, the strength ( $B$ ) and frequency of the magnetic field typically used were around  $\sim 50$  gauss (dependent on magnetic material) and  $\sim 50$  Hz, respectively. Even if we assume  $\Omega_2 = 50$  Hz, for an increase in viscosity by a factor of 2 (for completely undiluted blood), the operational magnetic field would have to be 100 gauss, which was well within the capabilities of the experimental setup.

In the following section, we discuss our observations on the motion of nanopropellers in blood at the lowest dilution (1.8 $\times$ ) attempted in these experiments. We observed a strong dependence of the propulsion efficiency on the position of the propeller in the experimental chamber. Under the action of a rotating magnetic field, it was always possible to rotate the propeller about its long axis (assuming the direction of magnetization to be along the short axis); however, the speed of the translational motion depended strongly on the position of the propeller, which in turn was determined by changing the focus of the microscope objective. The speed was found to be extremely low when the propeller was situated in a region between the glass coverslip and the blood cells (see Supporting Information movie M3) but was significantly higher when the propeller was in between the blood cells (see Supporting Information movie M1 or M4). The possible positions of the propellers in the experimental chamber, along with a plot of their displacement as a function of time are shown in Figure 4A. The strong position dependence was probably due to the hydrodynamic effects of the proximity of a hard wall (cover glass) as opposed to well-dispersed blood cells, and the corresponding difference in the hydrodynamic flow fields. A quantitative understanding of this phenomenon would require a detailed numerical model, which is beyond the scope of the present manuscript.

Unlike simple Newtonian fluids like deionized water or model biofluids (e.g., PBS, SBF), the composition of human blood is highly heterogeneous, which in a first approximation, can be considered a dispersion of colloidal structures (red and white blood cells, etc.) in a fluid (plasma). Although the velocity of nanopropellers in simple fluids was constant with some fluctuations<sup>35</sup> arising from thermal noise, the motion in blood showed an interesting stick-slip dynamics, which was evident from the motion of the propellers in movies M1 and M4. We believe this to be related to colloidal jamming<sup>36,37</sup> and subsequent unjamming, of the blood cells. The behavior has been highlighted in the insets of Figure 4B, where the displacement of the propeller has been plotted as a function of time, obtained by analyzing the movie M4 (dilution 1.8 $\times$ ). The displacement varied linearly with time until the blood cells were jammed by the forward fluid flow induced by the propeller, at which point the thrust generated was not enough to overcome the drag. The colloidal unjamming typically occurred after about 1–2 s, following which the propeller was able to move again with a constant velocity. The origin of the observed stick-and-slip motion is related to the multi-component nature of blood, which is inherently related to its non-Newtonian<sup>38</sup> behavior. Previous studies of nanomotors in

blood were conducted at much higher dilutions and, therefore, were not susceptible to similar jamming effects.

Next, we discuss the frequency dependence of the motion of propellers in blood. The results are shown in Figure 4C, where an approximate linear dependence of the velocity on the rotational frequency could be observed with achieved speeds as high as 15  $\mu\text{m}/\text{s}$ . In all these measurements, the propellers went through the space in between the blood cells, as can be seen from the movie shared in the Supporting Information (movie M4), taken at magnetic field frequency of 85 Hz. The hydrodynamic pitch was similar to what was obtained in water, as shown in the same graph. By appropriate choice of geometry and magnetic material, it may be possible to achieve propeller speeds greater than blood flow rates ( $>100$   $\mu\text{m}/\text{second}$ <sup>39,40</sup>) in capillaries, which could be of relevance to *in vivo* studies.

Finally, we discuss the cytocompatibility properties of the ferrite-coated propellers, relevant for the ambitious *in vivo* applications envisioned with nanovoyagers. The C2C12 murine myoblast cell line was used as a model cell line, as these cells exhibit a distinct morphology in their differentiated and undifferentiated state. Additionally, the same cell line has been recently used for the demonstration of cytocompatibility of magnetic propellers based on SU8-NiTi<sup>20</sup>, SU8-magnetite<sup>41</sup>, and photoresist-Fe.<sup>42</sup> In the present study, we have used MTT biochemical assay to quantify the mitochondrially active viable cells and the fluorescence microscopy observations to study the cell morphology. The samples under study were (A)  $\text{SiO}_2$  helices without any magnetic material or ferrite coating, (B)  $\text{SiO}_2$  helices with a ferrite coating, (C)  $\text{SiO}_2$  helices with Fe, (D)  $\text{SiO}_2$  helices with Co, (E)  $\text{SiO}_2$  helices with Fe and a ferrite coating, (F)  $\text{SiO}_2$  helices with Co and a ferrite coating, along with (G) a glass coverslip as the control sample. The results of the MTT assay (details in Materials and Methods section) of these samples are shown in Figure 5A, where the number of C2C12 mouse myoblast cells systematically increased on each sample (except the silica helices with Co-coatings), over different time scales in culture up to 72 h. This clearly indicates that all the substrates promote myoblast proliferation over 3 days in culture. Importantly, the cell viability of samples A, B, C, E were similar to the control sample G, thus implying good cytocompatibility (see Figure 5) of the ferrite-coated nanopropellers and those which have iron as the underlying magnetic material. On the other hand, cobalt is identified as highly toxic to living cells, accounting for the very low cell viability (down to 15% on day 3) on cobalt-coated propellers (sample D) without a conformal coating. Once coated with the ferrite (sample F), the toxicity due to cobalt was reduced but was still significantly higher than in the control sample. In addition, the O.D. was found to increase systematically, although it was still less than the control. This may also provide evidence for the leaching of Co in the medium, which decreases in the presence of the coating. This was also evident from the energy dispersive spectrum (data shown in Table 1). From the cell viability results, one of the points that can be concluded is that the ferrite coating reduces Co leaching. The studies on Co toxicity suggest that Co causes DNA strand breaks due to the generation of active reactive oxygen species (ROS), as Co is known<sup>43</sup> to be cytotoxic. This trend is clearly seen in the MTT results (see Figure 5).

In order to further confirm any adverse effect on the morphology of the cultured cells (sample E), we studied the morphology and spreading of the myoblast cells on the

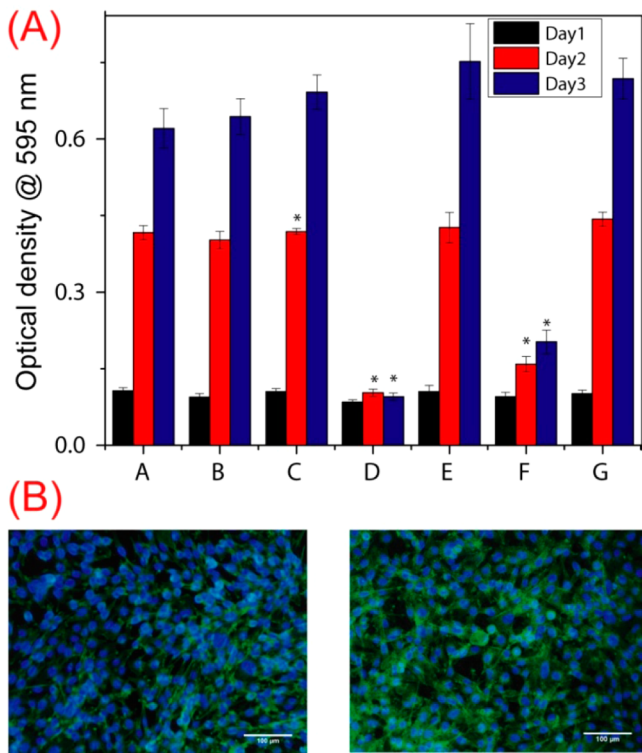


**Figure 5.** (A) Results of the MTT assay for different samples, corresponding to (A)  $\text{SiO}_2$  helices without any magnetic material or ferrite coating, (B)  $\text{SiO}_2$  helices with a ferrite coating, (C)  $\text{SiO}_2$  helices with Fe, (D)  $\text{SiO}_2$  helices with Co, (E)  $\text{SiO}_2$  helices with Fe and a ferrite coating, (F)  $\text{SiO}_2$  helices with Co and a ferrite coating, along with (G) tissue culture polystyrene as control sample. (B) Fluorescence images of cellular growth above silica (left) and ferrite-coated (right) samples. See Materials and Methods section for more details (\* represents statistical significance with respect to the control,  $p < 0.05$ ).

substrate using fluorescence microscopy. To visualize the details of cytoskeletal structures and the shape of the nuclei, myoblasts were immunostained for F-actin and counterstained with Hoechst stain for nuclei visualization after 3 days of incubation. As shown in the fluorescence images in Figure 5B, the cellular morphology on day 3 for ferrite-coated samples were as good as in the control sample. The characteristic spindle-like morphology, typical of myoblast cells was clearly visible. An investigation of cellular adhesion to the substrate as observed by scanning electron microscopy also confirms these observations (see Supporting Information).

On the basis of the MTT assay, fluorescence microscopy, and SEM imaging, it can be concluded that the conformal ferrite coatings are cytocompatible and promote cell adhesion and proliferation of C2C12 myoblast cells.

## CONCLUSION

We have developed a system of cytocompatible nanopropellers that can be maneuvered in various biological fluids with a small and homogeneous rotating magnetic field. The method of actuation is noninvasive, does not require any chemical fuel, and is therefore ideally suited for *in vivo* applications. We have demonstrated for the first time that the nanovoyagers can be actuated in human blood at negligible dilutions. An interesting stick-and-slip motion was observed in these *in vitro* studies, which was related to the colloidal jamming of the blood cells.

Obtaining a conformal ferrite coating was a crucial step of this study, which can be incorporated in various other designs of nanomotors as well. The cell culture experiments also establish the cytocompatibility property of the Fe/ferrite based coatings with myoblast cells *in vitro*. Interestingly, ferrites display large magnetic hysteresis (and therefore large specific absorption rate), implying that the present system can be readily used in applications pertaining to magnetic hyperthermia.<sup>44</sup> It will be interesting to see if this and various other *in vivo* biological applications can be realized with this powerful system of magnetic nanovoyagers.

## MATERIALS AND METHODS

**Fabrication of Nanopropellers.** For the fabrication of nanopropellers, we use a Langmuir–Blodgett trough (Apex Instruments) to self-assemble a monolayer of polystyrene beads (diameter 1  $\mu\text{m}$ , Spherotech Inc.) assembled on a Si wafer. This is followed by plasma etching using a plasma cleaner (Harrick Plasma) for a few minutes to reduce the bead diameter and thereby increase the spacing between the beads. The monolayer layer acts as the template<sup>45</sup> for the fabrication of nanopropellers using glancing angle deposition (GLAD) as shown in Figure 1A. Following the fabrication, the propellers are sonicated and laid down on a cleaned Si wafer and a layer of ferromagnetic material (Co or Fe) is deposited over them to render them magnetic.

**Different Solutions under Study.** Phosphate-buffered saline (PBS) and simulated body fluid (SBF) were prepared according to the standard recipe. Fetal bovine serum (FBS) was obtained from a commercial source (Invitrogen). The studies with blood were carried out using fresh human blood after adding EDTA to it.

**Synthesis of Various Types of Coatings.** *Zinc Ferrite Coating.* The typical procedure employed for the synthesis of nanoparticles of ZFO by the microwave-assisted chemical process<sup>46</sup> is as follows. Metal–organic precursors  $\text{Zn}(\text{acac})_2$  and  $\text{Fe}(\text{acac})_3$  were purchased from Merck and used as received. Stoichiometric (1:2) amounts of these precursors (0.5 mmol of  $\text{Zn}(\text{acac})_2$  and 1 mmol of  $\text{Fe}(\text{acac})_3$ ) were added to 15 mL of ethanol sequentially and stirred gently for a couple of minutes to obtain a clear solution of the precursor materials. An aliquot of 25 ml of 1-decanol was added and mixed thoroughly thereafter. The substrate containing nanopropellers was placed in the tube. The reaction mixture was irradiated in a microwave oven (2.45 GHz, 300 W, 1.5 min) fitted with a water-cooled reflux condenser to avoid the loss of solvent during the reaction. Following the reaction, the substrate was taken out and washed with ethanol to remove the unreacted mixture. Various thicknesses of zinc ferrite coatings, ranging from 50 to 250 nm, could be obtained by altering process parameters suitably.

*Silica Coating.* Silicon dioxide coating was deposited on the propellers by plasma enhanced chemical vapor deposition. The process was carried out at 350 °C at 1 Torr using nitrous oxide as the oxidizer and silane gas as precursor. The thickness of the silica layer was about 100 nm.

*Alumina Coating.* Alumina coating on the propellers was obtained using atomic layer deposition. The process was carried out at 135 °C using triethyl aluminum and deionized water as precursors. The thickness of the alumina layer obtained through 125 ALD “cycles” was about 100 nm. Prior to the alumina coating, the polystyrene was removed by oxygen plasma, so as not to contaminate the ALD chamber.

**Titanium Coating.** Titanium was sputter-deposited on the propellers using a commercial coater (Anelva Sputtering Unit Model SPF-332H) at a typical rate of 0.5 nm/second. The thickness of the Ti film was about 100 nm.

**Gold and Silver Coating.** Gold and silver coatings were deposited on the propellers separately for different sets of experiments using thermal evaporator at a vacuum of  $5 \times 10^{-5}$  mbar at a typical rate of 10 nm/second. The thicknesses of gold and silver layers were about 100 nm.

**Characterization Techniques.** The morphology of the coating and that of the propellers was characterized using scanning electron microscopy (Carl Zeiss). The surface composition was analyzed using energy dispersive X-ray spectrometry (EDS).

**Biocompatibility Study. Cell Culture.** The C2C12 murine myoblast line was used for all in vitro experiments. Cryopreserved C2C12 cells were procured from National Centre for Biological Science (NCBS), Bangalore. Cells were expanded in complete media containing Dulbecco's modified Eagle's medium (DMEM; Invitrogen) supplemented with 15% fetal bovine serum (FBS; Invitrogen), 1% antibiotic antimycotic solution (Sigma) and 2 mM L-glutamine (Invitrogen). Cells were incubated (Sanyo, MCO-18AC, U.S.A.) in an atmosphere of 5% CO<sub>2</sub> at 37 °C. Cells were used for further experiments after harvesting them with 0.05% trypsin-EDTA (Invitrogen) after they reached 70–80% confluence and subcultured for further experiments. Cells with a passage number less than 20 were used. Cell density was counted using a manual hemocytometer (Rohem, India) and media change was done every two days. All the samples were sterilized under UV light for 12 h after washing them with PBS and ethanol.

**MTT Assay.** The MTT assay was used to evaluate cell viability. The MTT reagent (3(4,5-dimethylthiazol-2-yl)-2,5-diphenyltetrazolium bromide, Sigma) gives an estimate of the metabolically active cells due to the formation of purple-colored formazan crystals by reduction. Approximately 4000–5000 cells/well were seeded on the sterilized samples placed in 24 well plates and incubated for 1, 2, and 3 days in CO<sub>2</sub> at 37 °C. Tissue culture polystyrene surface was used as the control. After the stipulated incubation period, the medium in the well plate was aspirated and washed twice with PBS, followed by the addition of 15% MTT stock (5 mg MTT reagent/mL PBS) in serum-free medium without phenol red. After incubation for 3 h, the purple-colored formazan crystals developed in the cells were solubilized using 0.5 mL DMSO (Merck) and the optical density was measured in a microplate reader (iMark, Biorad laboratories, India) at 595 nm, with a reference wavelength of 750 nm. Cell viability was calculated from the ratio of the average absorbance on the sample to the average absorbance of the control. The MTT assay was repeated three times.

**Cell Morphological Analysis.** Cell proliferation and orientation of the C2C12 mouse myoblast cells were studied using fluorescence microscopy (Nikon Eclipse, model LV100D, Japan). C2C12 cells were grown on sterile samples and on a glass coverslip (control) for three days. After three days, the medium was aspirated, the cells were washed with PBS and then fixed with 4% paraformaldehyde (PFA). PFA was removed and the cells were washed after 20 min. Cells were permeabilized by treatment of the samples with 0.1% Triton X solution for 8–10 min. The samples were again washed with PBS and were treated with 1% FBS to prevent nonspecific binding of fluorescent dyes. Actin filaments were stained with Alexa Fluor 488 (Invitrogen) for 20 min and cell nuclei were

stained with Hoechst stain 33342 (Invitrogen). Cell density was calculated using Image J software from at least five images for each sample.

**Statistical Analysis.** Statistical analysis was performed with SPSS-20.0 software (IBM, U.S.A.) using mixed model two-way ANOVA followed by Bonferroni's posthoc test. The analyzed data were plotted as mean  $\pm$  standard error. Values of  $p < 0.05$  were considered as statistically significant.

## ■ ASSOCIATED CONTENT

### S Supporting Information

Description of the movies M1, M2, M3, and M4 and experimental details on cell adhesion studies and morphological analysis. This material is available free of charge via the Internet at <http://pubs.acs.org>.

## ■ AUTHOR INFORMATION

### Corresponding Authors

\*P. L. Venugopalan. E-mail: lekshmy@cense.iisc.ernet.in.

\*A. Ghosh. E-mail: ambarish@ece.iisc.ernet.in.

### Notes

The authors declare no competing financial interest.

## ■ ACKNOWLEDGMENTS

The authors thank Arijit Ghosh for helpful discussions, Suhana Sarangi and Raghav Gupta for help with the ferrite coatings, Vaisakh Vadakkumbatt and Suman Karmakar for help with the biofluids, Debadrita Paria for help with the image analysis, and facility technologists at the N<sup>2</sup>FC for their help with the alumina, silica, and titanium coatings. The usage of the facilities in Micro and Nano Characterization Facility (MNCF, CeNSE) at IISc, and funding from the Department of Biotechnology is gratefully acknowledged. This work is partially supported by the Ministry of Communication and Information Technology under a grant for the Centre of Excellence in Nanoelectronics, Phase II. P.L.V. thanks the Department of Science and Technology for financial assistance through the INSPIRE Fellowship (IF 120503).

## ■ REFERENCES

- (1) Feynman, R. P. *J. Microelectromech. Syst.* **1992**, *1*, 60–66.
- (2) Wang, J. *ACS Nano* **2009**, *3*, 4–9.
- (3) Wang, J. *Nanomachines: Fundamentals and Applications*; Wiley-VCH: Weinheim, Germany, 2013.
- (4) Wang, J.; Gao, W. *ACS Nano* **2012**, *6*, 5745–5751.
- (5) Ebbens, S. J.; Howse, J. R. *Soft Matter* **2010**, *6*, 726–738.
- (6) Fischer, P.; Ghosh, A. *Nanoscale* **2011**, *3*, 557–563.
- (7) Ashkin, A. *Biophys. J.* **1992**, *61*, 569–582.
- (8) Gosse, C.; Croquette, V. *Biophys. J.* **2002**, *82*, 3314–3329.
- (9) Fournier-Bidoz, S.; Arsenault, A. C.; Manners, I.; Ozin, G. A. *Chem. Commun.* **2005**, 441–443.
- (10) Paxton, W. F.; Kistler, K. C.; Olmeda, C. C.; Sen, A.; St. Angelo, S. K.; Cao, Y.; Mallouk, T. E.; Lammert, P. E.; Crespi, V. H. *J. Am. Chem. Soc.* **2004**, *126*, 13424–13431.
- (11) Gao, W.; Uygun, A.; Wang, J. *J. Am. Chem. Soc.* **2012**, *134*, 897–900.
- (12) Solovev, A. A.; Mei, Y.; Bermúdez Ureña, E.; Huang, G.; Schmidt, O. G. *Small* **2009**, *5*, 1688–1692.
- (13) Kagan, D.; Benchimol, M. J.; Claussen, A. J.; Chuluun-Erdene, E.; Esener, S.; Wang, J. *Angew. Chem., Int. Ed.* **2012**, *51*, 7519–7522.
- (14) Gao, W.; Pei, A.; Wang, J. *ACS Nano* **2012**, *6*, 8432–8438.
- (15) Calvo-Marzal, P.; Sattayasamitsathit, S.; Balasubramanian, S.; Windmiller, J. R.; Dao, C.; Wang, J. *Chem. Commun.* **2010**, *46*, 1623–1624.

- (16) Ishiyama, K.; Sendoh, M.; Arai, K. *I. J. Magn. Magn. Mater.* **2002**, 242–245 (Part 1), 41–46.
- (17) Sato, F.; Jojo, M.; Matsuki, H.; Sato, T.; Sendoh, M.; Ishiyama, K.; Arai, K. I. *IEEE Trans. Magn.* **2002**, 38, 3362–3364.
- (18) Ghosh, A.; Fischer, P. *Nano Lett.* **2009**, 9, 2243–2245.
- (19) Peyer, K. E.; Tottori, S.; Qiu, F.; Zhang, L.; Nelson, B. J. *Chem-Eur. J.* **2013**, 19, 28–38.
- (20) Tottori, S.; Zhang, L.; Qui, F.; Krawczyk, K. K.; Franco-Obregon, A.; Nelson, B. J. *Adv. Mater.* **2012**, 24, 811–816.
- (21) Xi, W.; Solovev, A. A.; Ananth, A. N.; Gracias, D. H.; Sanchez, S.; Schmidt, O. G. *Nanoscale* **2013**, 5, 1294–1297.
- (22) Zhang, L.; Abbott, J. J.; Dong, L.; Kratochvil, B. E.; Bell, D.; Nelson, B. J. *Appl. Phys. Lett.* **2009**, 94, 064107–3.
- (23) Zhang, L.; Petit, T.; Peyer, K. E.; Nelson, B. J. *Nanomed.: Nanotechnol., Biol. Med.* **2012**, 8, 1074–1080.
- (24) Garcia-Gradilla, V.; Orozco, J.; Sattayasamitsathit, S.; Soto, F.; Kuralay, F.; Pourazary, A.; Katzenberg, A.; Gao, W.; Shen, Y.; Wan, J. *ACS Nano* **2013**, 7, 9232–9240.
- (25) Wang, W.; Castro, L. A.; Hoyos, M.; Mallouk, T. E. *ACS Nano* **2012**, 6, 6122–6132.
- (26) Gao, W.; Feng, X.; Pei, A.; Kane, C. R.; Tam, R.; Hennessy, C.; Wang, J. *Nano Lett.* **2014**, 14, 305–310.
- (27) Soler, L.; Martinez-Cisneros, C.; Swiersy, A.; Sanchez, S.; Schmidt, O. G. *Lab Chip* **2013**, 13, 4299–4303.
- (28) Zhao, G.; Viehrig, M.; Pumera, M. *Lab Chip* **2013**, 13, 1930–1936.
- (29) Hawkeye, M. M.; Brett, M. J. *J. Vac. Sci. Technol., A* **2007**, 25, 1317–1335.
- (30) Mandal, P.; Ghosh, A. *Phys. Rev. Lett.* **2013**, 111, 248101–5.
- (31) Bouchard, L. S.; Anwar, M. S.; Lui, G. L.; Hann, B.; Xie, Z. H.; Gray, J. W.; Wang, X.; Pines, A.; Chen, F. F. *Proc. Natl. Acad. Sci. U. S. A.* **2009**, 106, 4085–4089.
- (32) Keaveny, E. E.; Walker, S. W.; Shelley, M. J. *Nano Lett.* **2013**, 13, 531–537.
- (33) Ghosh, A.; Mandal, P.; Karmakar, S.; Ghosh, A. *Phys. Chem. Chem. Phys.* **2013**, 15, 10817–10823.
- (34) Ghosh, A.; Paria, D.; Singh, H. J.; Venugopalan, P. L.; Ghosh, A. *Phys. Rev. E* **2012**, 86, 031401–5.
- (35) Ghosh, A.; Paria, D.; Rangarajan, G.; Ghosh, A. *J. Phys. Chem. Lett.* **2013**, 5 (1), 62–68.
- (36) Fuchs, M.; Cates, M. E. *Phys. Rev. Lett.* **2002**, 89, 248304–8.
- (37) Nordstrom, K. N.; Verneuil, E.; Arratia, P. E.; Basu, A.; Zhang, Z.; Yodh, A. G.; Gollub, J. P.; Durian, D. J. *Phys. Rev. Lett.* **2010**, 105, 175701–4.
- (38) Chien, S.; King, R. G.; Skalak, R.; Usami, S.; Copley, A. L. *Biorheology* **1975**, 12, 341–346.
- (39) Bollinger, A.; Butti, P.; Barras, J. P.; Trachsler, H.; Siegenthaler, W. *Microvasc. Res.* **1974**, 7, 61–72.
- (40) Stücker, M.; Baier, V.; Reuther, T.; Hoffmann, K.; Kellam, K.; Altmeyer, P. *Microvasc. Res.* **1996**, 52, 188–192.
- (41) Suter, M.; Zhang, L.; Siringil, E. C.; Peters, C.; Luehmann, T.; Ergeneman, O.; Peyer, K. E.; Nelson, B. J.; Hierold, C. *Biomed. Microdevices* **2013**, 15, 997–1003.
- (42) Qiu, F.; Zhang, L.; Peyer, K. E.; Casarosa, M.; Franco-Obregon, A.; Choi, H.; Nelson, B. J. *J. Mater. Chem. B* **2014**, 2, 357–362.
- (43) Gault, N.; Sandre, C.; Poncy, J. L.; Moulin, C.; Lefaix, J. L.; Bresson, C. *Toxicol. In Vitro* **2012**, 24, 92–98.
- (44) Sharifi, I.; Shokrollahi, H.; Amiri, S. *J. Magn. Magn. Mater.* **2012**, 324, 903–915.
- (45) Venugopalan, P. L.; Gupta, G.; Ghosh, A.; Singh, H. J.; Ghosh, A. *Int. J. Polym. Mater. Polym. Biomater.* **2013**, 62, 499–501.
- (46) Sai, R.; Kulkarni, S. D.; Vinoy, K. J.; Bhat, N.; Shivashankar, S. A. *J. Mater. Chem.* **2012**, 22, 2149–2156.